Tailoring of Mesenchymal Stem Cells Behavior on Plasma-Modified Polytetrafluoroethylene

*Huaiyu Wang, Dixon T. K. Kwok, Ming Xu, Haigang Shi, Zhengwei Wu, Wei Zhang, and Paul K. Chu**

Bone loss related to osteoporosis, trauma, cancer, and congenital abnormalities continues to be a serious problem in the medical field. Nowadays, over 2 million bone repair or replacement procedures are carried out worldwide[1] and the annual orthopedic cost is tens of billions of dollars.[2] Alloplastic nonbiological implants are commonly used in the treatment of bone damages as an alternative to autologous grafts. However, conventional artificial implants tend to induce the formation of neighboring soft tissues rather than direct bone integration, resulting in fibrous encapsulation of the implant materials.[3,4] This degrades the quality of non-load-bearing artificial prostheses and even leads to failure of load-bearing implants *via* micromotion. Consequently, development of advanced materials not only tolerated by the body but also capable of bone integration is vital to the success of orthopedic implants.

Integration of implants with native bones, a process termed osseointegration, involves both osteoconduction and osteoinduction. Osteoconduction is the process in which osteoblasts migrate and sprout from the surrounding tissues onto the implants whereas osteoinduction refers to bone formation induced *de novo* by triggering stem cell differentiation into the osteoblastic lineage.[2,5,6] Hence, artificial materials for bone replacement are typically tested with osteoblasts or stem cells before clinical acceptance. Compared to evaluations employing osteoblasts, characterization with stem cells is more meaningful as the osteoinduction process is essential, especially for large critical-size bone repair.

Among the various types of stem cells, mesenchymal stem cells (MSCs) derived from bone marrow and abundant in the skeletal tissues have attracted much interest in the *in vitro* qualification of orthopedic materials as they are the precursors of the entire osteoblastic lineage. MSCs are multipotent stem cells that can terminally differentiate into various lineages such as osteoblasts,[7] chondrocytes,[8,9] myocytes,[10] adipocytes,[11] and so on by generating the appropriate intermediate progenitors. They also possess other desirable properties such as hypoimmunogenicity as well as robust self-renewal capability.

It has been reported that the stem cell fate can be tailored by varying materials properties such as chemistry,[12,13] elasticity,[14] and surface topography.[3,15–17] Curran et al. and Benoit et al. independently demonstrated that amino[12] and phosphate[13] functionalization of biomaterials had positive effects on osteogenesis of cultured MSCs. Engler et al. indicated that MSCs were sensitive to the substrate elasticity and capable of osteogenic differentiation on stiff substrates.[14] Dalby et al. embossed ordered or disordered nanoholes on polymethylmethacrylate (PMMA) and observed that disorder on the nanoscale could direct MSCs into the osteoblastic lineage.[3]

Here, we demonstrate the ability to tailor the behavior of mesenchymal stem cells on polytetrafluoroethylene (PTFE) by simple plasma modification. We have recently reported that oxygen plasma immersion ion implantation (O_2 PIII) can produce a superhydrophobic nanostructured surface capable of promoting the osteogenic behavior of primary osteoblasts.[18] By conducting different gas PIII and an optional second PIII process involving ammonia, different surface properties can be obtained selectively and locally on the PTFE to direct the adhesion, proliferation, and differentiation of MSCs.

The samples were processed using a special mesh-assisted plasma immersion configuration (Figure S1, Supporting Information) designed for insulating samples and the samples are named according to the processing parameters as shown in **Table 1**. Following sample preparation, scanning electron microscopy

Table 1. Main instrumental conditions.

Gas sources	Voltage [kV]	Pulse duration [μs]	Pulsing frequency [Hz]	Treatment time [min]	Sample names
Nil	Nil	Nil	Nil	Nil	U-P
Oxygen	–15	200	500	90	O-P
Oxygen	–15	200	500	90	OA(S)-P
Ammonia	–15	30	50	90	
Nitrogen	–15	200	500	90	N-P
Nitrogen	–15	200	500	90	NA-P
Ammonia	–15	200	500	90	
Hydrogen	–15	200	500	90	HA-P
Ammonia	–15	200	500	90	

Dr. H. Y. Wang, Dr. D. T. K. Kwok, Dr. M. Xu, Dr. Z. W. Wu, Prof. P. K. Chu
Department of Physics & Materials Science
City University of Hong Kong
Tat Chee Avenue, Kowloon, Hong Kong, China
E-mail: paul.chu@cityu.edu.hk
Dr. Z. W. Wu
Department of Modern Physics
University of Science and Technology of China
Hefei, Anhui, 230026, China
H. G. Shi, Dr. W. Zhang
Technical Institute of Physics and Chemistry
Chinese Academy of Sciences, Beijing, 100080, China

DOI: 10.1002/adma.201104967

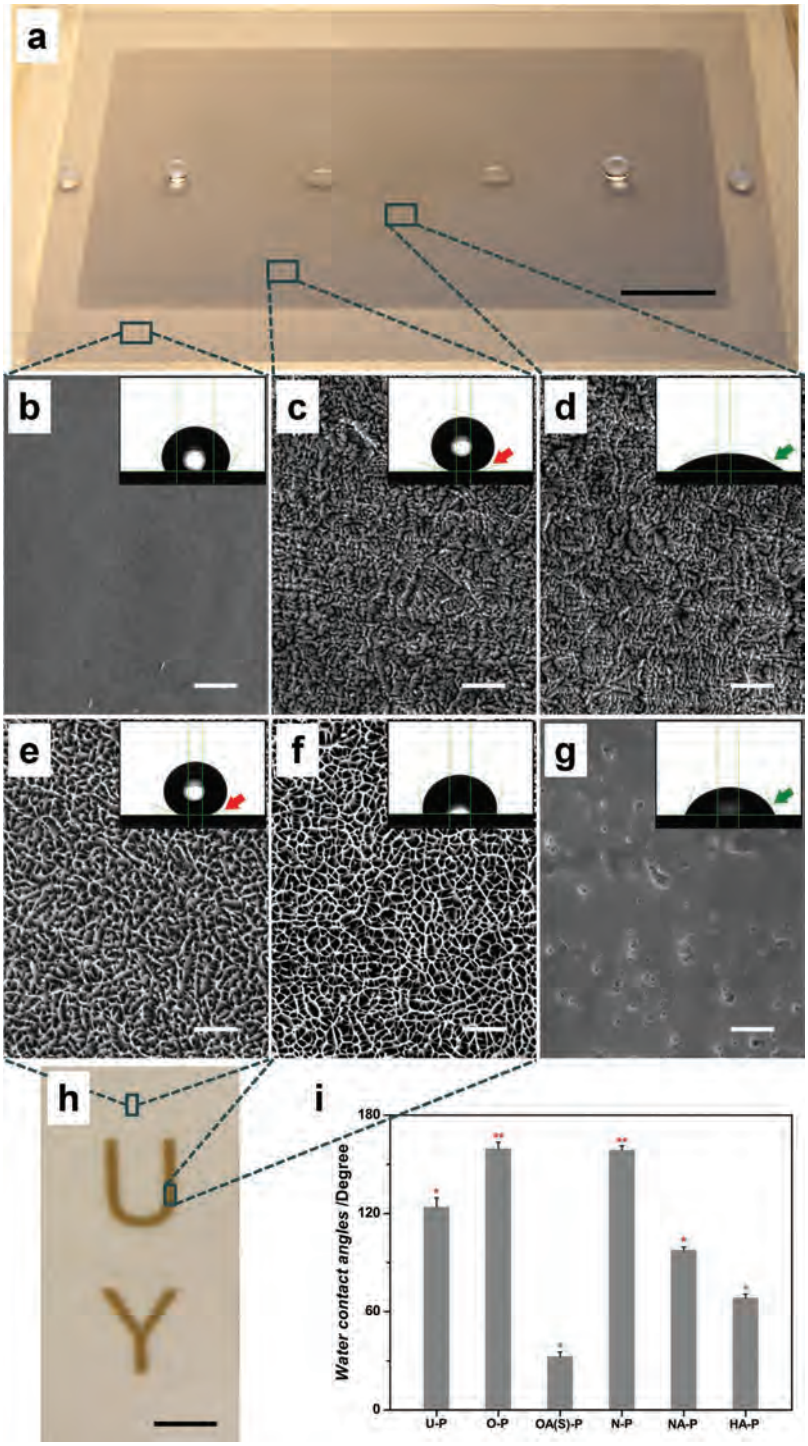

Figure 1. Macroscopic/microscopic aspects and hydrophilicity of the samples. a, Oblique view of PTFE with symmetrical regional PIII treatments and the water droplets on it, note the various appearances of water droplets (scale bar is 1 cm). b-g, SEM images (top view) of the samples designated as (b) U-P, (c) O-P, (d) OA(S)-P, (e) N-P, (f) NA-P, and (g) HA-P with typical water droplet images inserted on the top-right, green arrows referred to the hydrophilic surface and red arrows referred to the superhydrophobic surface (scale bar is 2 μm). h, Photograph (top view) of PTFE with asymmetrical regional PIII treatments, note that the mask patterns are clearly imprinted onto the sample (scale bar is 5 mm). i, Water contact angles measured on the samples, green * referred to the hydrophilic surface, red * referred to the hydrophobic surface and red ** referred to the superhydrophobic surface.

(SEM) was performed to determine the surface topographies and the pristine PTFE (U-P) has a flat morphology as shown in **Figure 1**b. Nanoscale rods are observed on the surface of the plasma-modified samples O-P (Figure 1c) and OA(S)-P (Figure 1d). Crosslinking and pores are observed from N-P (Figure 1e) and NA-P (Figure 1f), respectively. The morphology of HA-P (Figure 1g) is similar to that of U-P with the addition of some shallow etched holes.

It is recognized that the surface hydrophilicity of biomaterials is crucial to their biofunctions such as cell adhesion and spreading. Hence, the hydrophilicity of the samples was evaluated by the static sessile drop method using distilled water as the medium and the images of the water droplets on the various samples are depicted in the top-right insets in Figures 1b-g. As indicated in Figure 1i, both O-P and N-P are superhydrophobic as the water contact angles (CA_{water}) are close to 160°, whereas NA-P (CA_{water} is 97.5°) and HA-P (CA_{water} is 68.4°) are relatively hydrophilic compared to U-P (CA_{water} is 123.8°). Interestingly, OA(S)-P, which possesses a surface morphology similar to that of the superhydrophobic sample O-P, is the most hydrophilic of all (CA_{water} is 32.5°). The difference is that OA(S)-P and NA-P undergo subsequent NH_3 PIII additionally compared to O-P and N-P. Our results illustrate that the surface hydrophilicity of the modified samples can be altered appreciably by using NH_3 plasma either with or without changing the surface morphology.

When the samples undergo PIII, the sample surfaces tend to react with the overlying plasma surrounding and substantial chemical shifts are created. As aforementioned, some functional groups such as amino groups enhance the osteogenesis of the cultured MSCs. Hence, X-ray photoelectron spectroscopy (XPS) which is a surface-sensitive characterization technique was employed to determine the surface chemistry which is vital to the MSCs functions. **Figures 2**a-d display the high-resolution XPS spectra acquired from various sample surfaces and the histogram of atomic percentages is displayed together in Figure 2e. In particular, U-P is abundant in C and F components with a C/F ratio of about 1/2 whereas O and N elements are undetectable. Compared to U-P, the C1s shift and F1s decrease are recognizable on O-P and N-P with the emergence of the O and N components (0.4% N on O-P and 2.3% N on N-P). The chemical alterations are more obvious on OA(S)-P and NA-P according to the prominent O and N appearance (8.3% N on OA(S)-P and 12.2% N on NA-P), C1s shift, and F1s decrease. For HA-P, the shift in the C1s binding energy

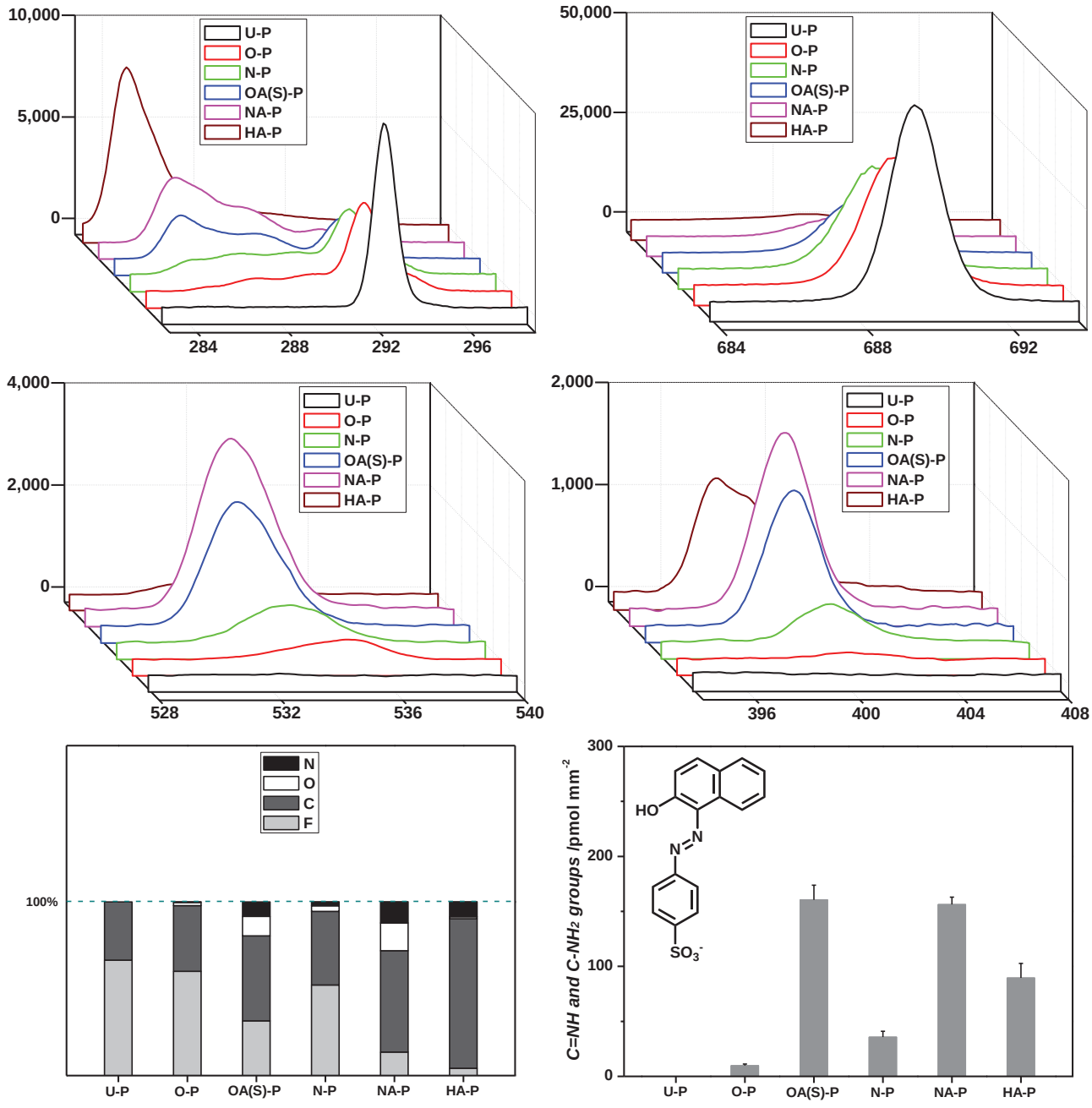

Figure 2. Surface chemistry of the tested samples. a-d, High resolution C1s (a), F1s (b), O1s (c) and N1s (d) spectra acquired from the surfaces of various samples. e, Atomic percentages of the various sample surfaces, note the similarities between O-P and N-P, and between OA(S)-P and NA-P. f, The C=NH/C–NH_2 density on the samples assayed by Orange II dye. The chemical structure of Orange II is inserted into the top-left and note the abundance of C=NH/C–NH_2 groups on OA(S)-P and NA-P.

is evident whereas F is barely detected. There is a substantial N component (8.6%) on HA-P and the binding energy shifts left obviously. It should be noted that no matter which kind of initial gas PIII is conducted, the samples after subsequent NH_3 PIII possess a large surface N concentration (>8%). This confirms that NH_3 PIII is quite different with the initial O_2 and N_2 PIII as it is more effective in boosting the surface nitrogen concentration. The high resolution C1s spectra are fitted and presented separately in **Figures 3**a-f for functional groups determination. Abundant CF_2 bonds (C_1 peak) are detected on U-P accompanied by few end groups (C'_1 peak). CF_2 bonds are also prominent on O-P and N-P when various functional groups such as C=O/C=NH (C_2 peak), C–OH/C–NH_2 (C_3 peak), and C–C/C=C (C_4 peak) appear. The end groups (C'_1 peak) on O-P and N-P are more significant compared to U-P. On OA(S)-P and NA-P, the C_2, C_3 and C_4 peaks are comparable to or even higher than the C_1 peak indicating drastic chemical variations. The C'_1 peaks on OA(S)-P and NA-P are also higher than that

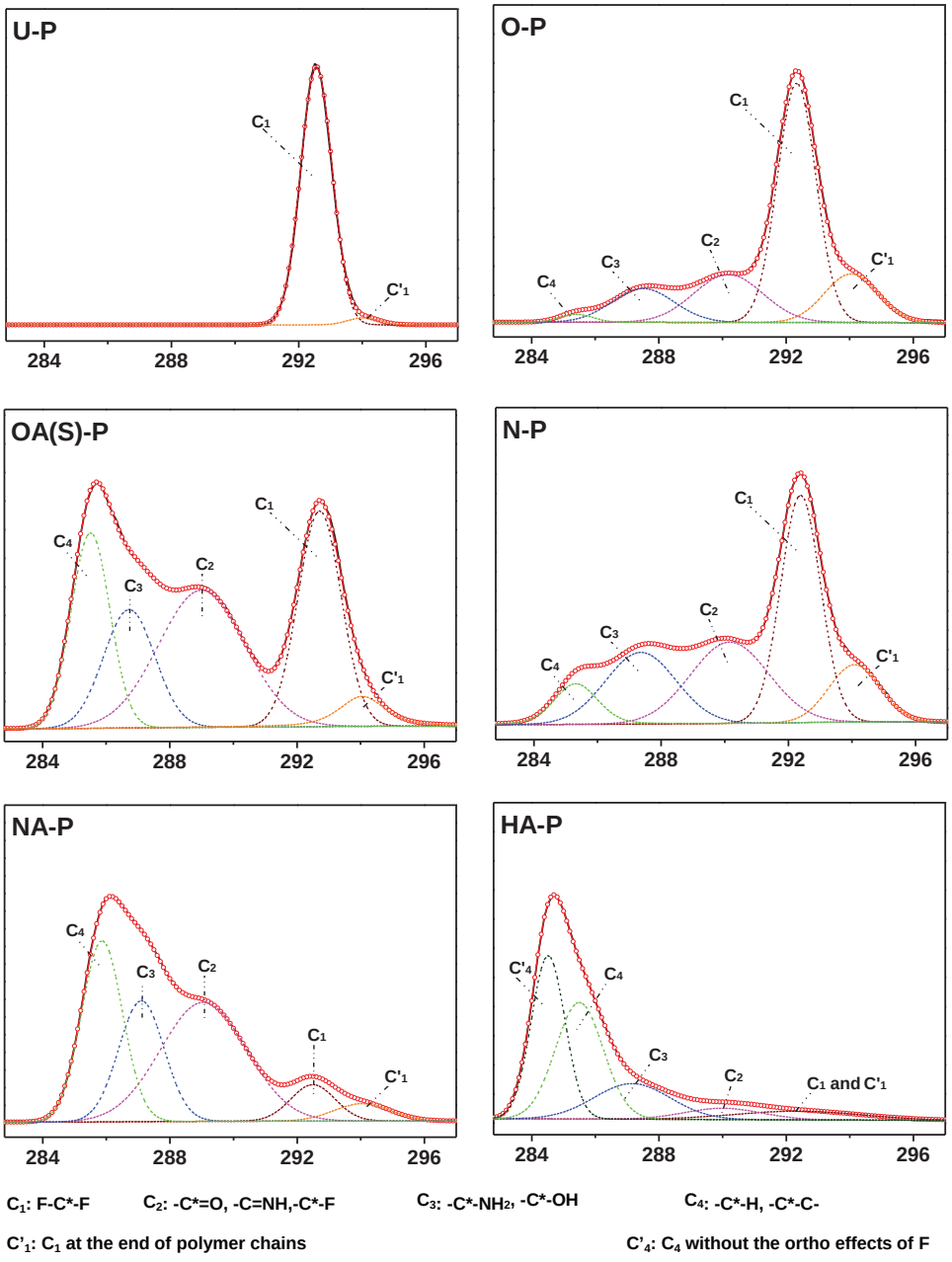

Figure 3. Surface chemistry of the tested samples. a-f,Fitted high resolution C1s spectra acquired from the surface of U-P (a), O-P (b), OA(S)-P (c), N-P (d), NA-P (e), and HA-P (f), bottom description referred to the attributions of fitted peaks.

on U-P. On HA-P, the chemical variation is the most drastic as the original C1s peaks related to the F component (C_1 and C'_1 peaks) are severely reduced and a new peak (C'_4 peak) with a lower binding energy emerges in response to the lack of F. HA-P has abundant C–C/C=C (C_4 and C'_4 peaks) and C–NH_2 bonds (C_3 peaks).

Since the N-containing groups are probably favorable to MSCs osteogenesis, a colorimetric assay using Orange II dye (chemical structure shown in the top-let inset in Figure 2f) was further performed to quantitatively determine the surface C=NH/C–NH_2 groups. This test serves as a supplement to the semiquantitative XPS measurements, and it is based on the fact that C=NH and C–NH_2 groups are electropositive under acidic conditions and they will adsorb electronegative dyes in an acidic solution and desorb them under alkaline conditions. As shown in Figure 2f, the C=NH/C–NH_2 groups on OA(S)-P and NA-P are more significant than the other samples when the C=NH/C–NH_2 density is above 150 pmol mm^{-2}. The C=NH/C–NH_2 density on HA-P (89.5 pmol mm^{-2}) is also larger than those on O-P (9.7 pmol mm^{-2}) and N-P (35.7 pmol mm^{-2}) whereas the C=NH/C–NH_2 density on U-P is below the detection limit. The colorimetric results demonstrate again that the PTFE samples

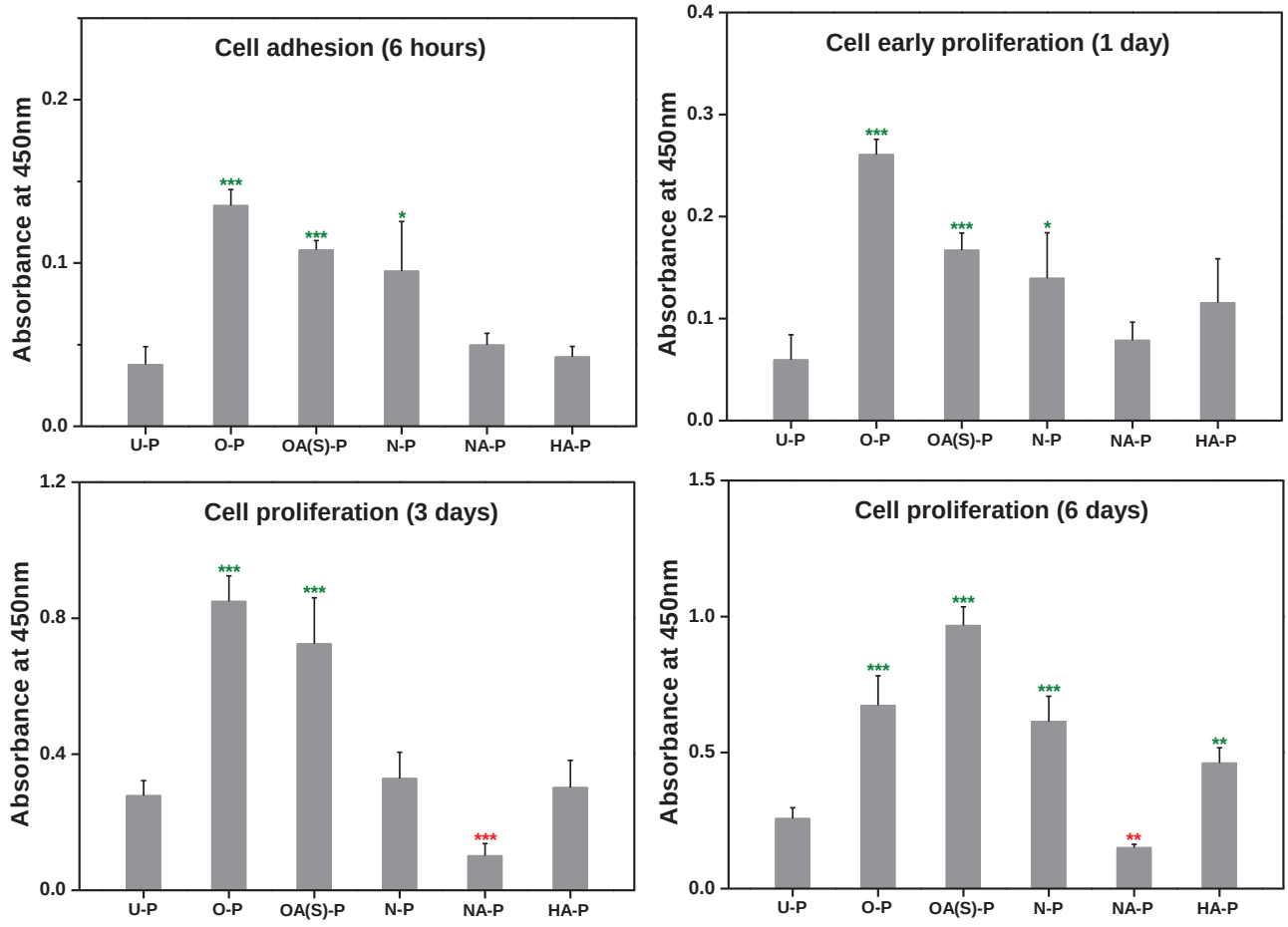

Figure 4. Time-dependent MSCs viabilities on the tested samples. a-d, MSCs adhesion (6 hours) (a) and 1 day (b), 3 days (c), 6 days (d) proliferation on the samples. Statistics evaluation is performed by ANOVA compared to U-P (indicated by *), * $p < 0.05$, ** $p < 0.01$, *** $p < 0.001$, green marks referred to the positive effects and red marks referred to the negative effects, note the positive effects of O-P, OA(S)-P and the negative effects of NA-P.

after undergoing subsequent NH_3 PIII treatments are rich with N-containing groups on their surfaces.

In the next step, the samples were incubated with MSCs to assess the roles of the various plasma treatments in supporting stem cell functions. The time-dependent viabilities of the cultured MSCs were first measured by a colorimetric assay WST-8, and the results reveal that both MSCs adhesion and early proliferation are best on O-P during the initial 24 hours of incubation (**Figure** 4a and 4b). After culturing for 3 days, MSCs proliferation on OA(S)-P is comparable to that on O-P and much better than that on other samples (Figure 4c). OA(S)-P shows the best MSCs proliferation alone after culturing for 6 days (Figure 4d). It should be noted that compared to U-P, only NA-P suppresses MSCs proliferation while other specimens support MSCs proliferation to a different extent.

Besides cells adhesion and proliferation, osteogenic differentiation of the cultured MSCs is crucial to the success of our samples as artificial implants since osteoinduction is involved. In this regard, the cultured MSCs was evaluated by quantitative real-time polymerase chain reaction (qPCR) with the primers for bone makers as the alkaline phosphatase activity (ALP, an enzyme regulating phosphate metabolism *via* hydrolyzing phosphate esters),[19,20] bone sialoprotein (BSP, a RGD containing phosphoprotein binding strongly with hydroxyapatite *via* a negatively charged domain),[21] osteopontin (OPN, a phosphoprotein serving as the bridge between the osteoblasts and hydroxyapatite),[22] and osteocalcin (OCN, a calcium binding protein regulating the bone crystal growth, the most specific marker in osteoblasts maturation).[23,24] The qPCR performance was divided into 2 groups. Firstly, the cells for qPCR determination were harvested from the substrates cultured in the osteogenic medium (total of 10 days with the initial 3 days cultured in a basic growth medium) and the MSCs on tissue culture polystyrene (TCPS) served as the control. Under these conditions, OA(S)-P reveals the most positive effects to osteogenic gene expressions. The ALP, BSP, and OCN levels are the highest on OA(S)-P and the OPN expression on OA(S)-P is higher than that on the control and comparable to that on other samples except U-P **(Figure 5**a-d). The osteogenic gene expressions were also assessed after culturing for 10 days in a basic growth medium, with the MSCs cultured on TCPS with or without osteogenic supplements serving as the negative and positive controls, respectively. As shown in **Figure 6**a-d, most of the tested samples are superior to the negative control showing

ADVANCED MATERIALS
www.advmat.de

www.MaterialsViews.com

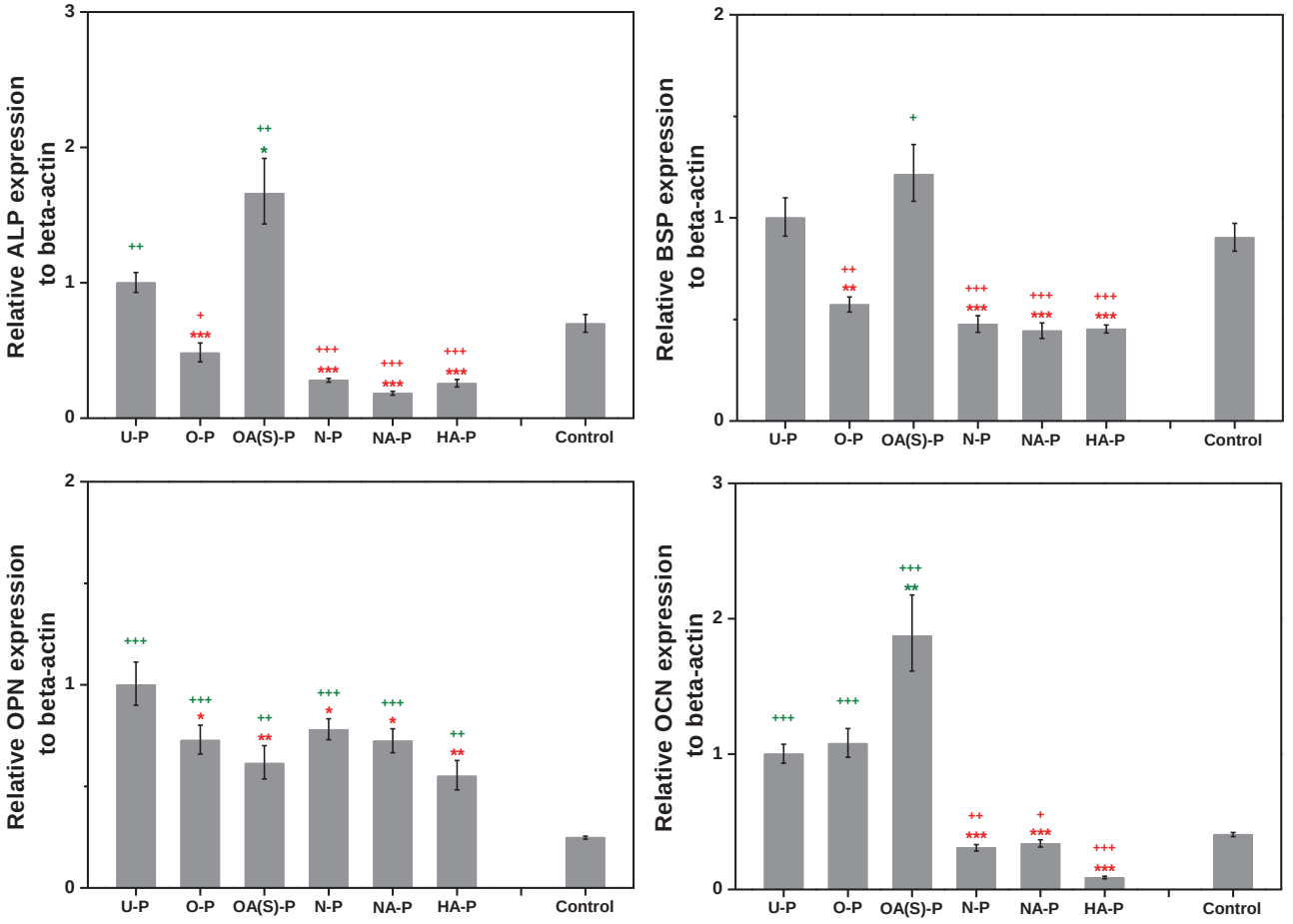

Figure 5. Differentiation of MSCs in the presence of osteogenic supplements. a-d, qPCR analysis of MSCs for (a) ALP, (b) BSP, (c) OPN, and (d) OCN after culturing for 10 days with TCPS with the same performance serving as the control. Statistical evaluation is performed by ANOVA compared to control (indicated by $^{+}$) and U-P (indicated by *), $^{+/*}$ $p < 0.05$, $^{++/**}$ $p < 0.01$, $^{+++/***}$ $p < 0.001$, green marks referred to the positive effects and red marks referred to the negative effects, note the up-regulation of ALP, BSP and OCN on OA(S)-P.

up-regulation of BSP, OPN, and OCN. More importantly, the osteogenic differentiation of MSCs on OA(S)-P is better than that on the positive control showing higher OPN expression and comparable ALP, BSP, and OCN levels. Sample O-P is also prominent in these gene expressions besides ALP down-regulation.

In addition to assessing the osteogenic gene expressions, 2 osteogenic proteins (OPN and OCN) were evaluated by immunofluorescent staining after the MSCs were cultured on the samples for 14 days in a basic medium. Figure 6e shows that both OPN and OCN staining of MSCs are recognizable on U-P (upper row) whereas OCN detection on NA-P is negligible (lower right). In contrast, the MSCs on OA(S)-P are more prominent in OCN staining (center right) than U-P and NA-P. The OPN and OCN immunofluorescent images of all the samples are shown together with hoechst staining in the same imaged area (Figure S2, Supporting Information). These observations are consistent with the qPCR results described above.

PIII is a simple and effective technique to fabricate different types of surface topographies on PTFE. Rods, crosslinking, and pores on the nanometer scale can be produced selectively together with other surface morphologies (Figure S3, Supporting Information). These various morphologies formed on PTFE are undoubtedly due to the complex reactions during PIII. There are two competitive reactions when polymers are treated with ion irradiation. One is chain scission when the atoms of polymer main-chains are displaced by the energetic ions (nuclear stopping) whereas the second one is branching/crosslinking which is due to the formation of free radicals by electronic excitation (electronic stopping).[25–27] In general, both reactions occur simultaneously, but one of them tends to dominate depending on the polymer types and irradiation conditions. It has been reported that PTFE in the solid state mainly undergoes chain scission during ion irradiation.[26–28] In particular, the C–F bonds of PTFE are high in energy and short in length and the adjacent F atoms are repulsive to each other due to Van der Waals force and steric effects. As a result, the polymer chains of PTFE are in a strain and the C–C bonds are weakened for facile scission. Furthermore, fluorine's electron-withdrawing nature determines that the electronic excitation of C atoms in PTFE is difficult and the resultant branching/crosslinking is infrequent. As shown in Figure 3, the obvious increase in the end groups (C'_1 peaks) on the modified samples is a clear evidence showing that PTFE undergoes chain scission

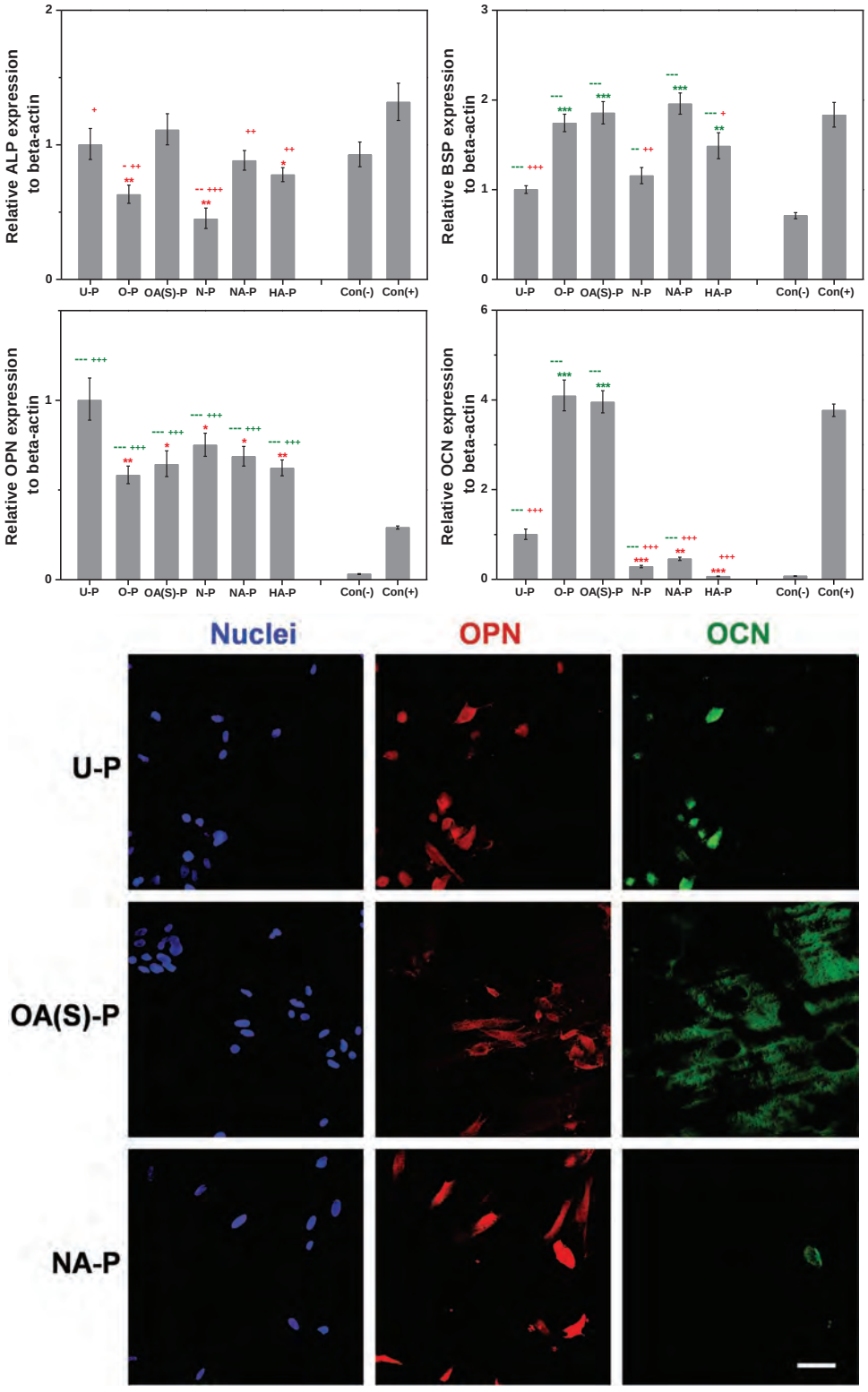

Figure 6. Differentiation of MSCs cultured in basic growth medium. a-d, qPCR analysis of MSCs for (a) ALP, (b) BSP, (c) OPN, and (d) OCN after culturing for 10 days with TCPS with the basic growth medium culture serving as con(–) and with the osteogenic medium culture serving as con(+). Statistical evaluation is performed by ANOVA as compared to con(–) (indicated by $^{-}$), con(+) (indicated by $^{+}$) and U-P (indicated by *), $^{-/+/*}$ $p < 0.05$, $^{--/++/**}$ $p < 0.01$, $^{---/+++/***}$ $p < 0.001$, green marks referred to the positive effects and red marks referred to the negative effects. It can be seen that the gene levels on OA(S)-P are comparable with or even higher than con(+). e, Immunofluorescent images of MSCs for OPN (center column) and OCN (right column) as well as hoechst staining (left column) after culturing for 14 days, note the most positive OCN stain on OA(S)-P (scale bar is 100 μm).

during gas PIII. The low C'_1 peak detected on HA-P is probably due to the lack of F atoms but not few end groups.

Besides changes in the surface topography, gas PIII is responsible for the chemical modification on the PTFE samples. SEM, contact angle measurements, XPS, and Orange II assay together disclose that the surface morphology of O-P and OA(S)-P is similar but their surface hydrophilicity and chemistry are drastically different. In this process, O_2 PIII produces the rod-shape morphology whereas the ensuing NH_3 PIII treatment mainly modulates the surface chemistry. The drastic shift from superhydrophobicity observed on O-P ($CA_{water} > 155°$) to hydrophilicity observed on OA(S)-P ($CA_{water} < 35°$) arises from the changes in surface chemistry and an amplification of surface roughness to CA appearance.[29] It should be noted that in addition to chemical modulation, NH_3 PIII is capable of producing further topographical alteration under different instrumental conditions (comparing N-P to NA-P). The parameters used in the ensuing NH_3 PIII are chosen to vary the surface chemistry with or without topographical alteration. It serves to selectively tailor the sample surfaces to enable a systematic investigation on the relationship between the surface properties and MSCs functions.

It is well known that serum used in the culturing of eukaryotic cells consists of many extracellular matrix proteins as albumin and fibronectin. These proteins play major roles in cell adhesion as they tend to aggregate on the substrates then promote the cell adhesion and proliferation, the protein aggregations for subsequent cell activities are typically about tens of nanometers in size.[17] The cell viability assay in this study furnishes evidence that O-P and OA(S)-P provide the positive cues in supporting MSCs adhesion and proliferation whereas NA-P is the least desirable substrate for MSCs proliferation. From the aspect of surface properties, OA(S)-P is similar to O-P in surface topography while its surface chemistry is closer to NA-P (abundant in C–NH_2 and C=NH groups) than O-P. It is a proof to that the surface topography of substrates is more essential than surface chemistry for the adhesion and proliferation of MSCs. As shown in Figures 1c, d and f, both the dimension and geometry of NA-P are different from those of O-P and OA(S)-P. The pores on NA-P with a spacing of up to 400 nm are probably too large for the protein aggregation to fill up and the sharp edges of the pores that can be anchored are limited in area. In contrast to NA-P, the rods on O-P and OA(S)-P are smaller in dimension (about 200 nm) and the geometrical feature of rods determines that protein aggregations are capable of anchoring on the troughs between the adjacent rods. The adhesion and proliferation of MSCs are promoted as a result. Our results are in line with the studies by Park et al. and Oh et al. that the MSCs adhesion and proliferation on small TiO_2 nanotubes (15[15] and 30[17] nm in diameter) are better than those on 100 nm TiO_2 nanotubes. It was pointed out in their reports that small TiO_2 nanotubes were superior to 100 nm TiO_2 nanotubes for proteins aggregating on and favored protein aggregations served as the key factor for the enhanced MSCs adhesion and proliferation.

In addition to the favorable properties supporting MSCs subsistence, OA(S)-P demonstrates the outstanding ability to direct MSCs differentiation into the osteogenic lineage. In most of the publications about biomaterials supporting MSCs functions, *in vitro* osteogenic differentiation of MSCs always relies on the biological intervention of additional inducing agents such as dexamethasone and glycerophosphate.[15,30,31] However, these osteogenic reagents are not intrinsic to the human body and it is difficult to distinguish whether the osteogenic effects arise solely from the samples or not. In this study, MSCs osteogenic differentiation is achieved on OA(S)-P in the presence of osteogenic supplements (Figure 5) or not (Figure 6). The results acquired are thus more trustworthy. As indicated by the qPCR performance in the basic medium culture, OA(S)-P is better than the other samples and even the positive control (osteogenic additions) in supporting MSCs osteogenesis. The performance is superior to that reported by Dalby et al.[3] and Oh et al.[17] that the osteogenic potentials of substrates are close to but not as good as that with osteogenic stimulins. Besides the most outstanding OA(S)-P, it is clear from qPCR and immunofluorescence results that O-P is also prominent in supporting MSCs osteogenesis with respect to the high expression of OCN/BSP gene (Figure 6) and the positive staining of OCN proteins (Figure S2, Supporting Information) in the absence of osteogenic additions. It is believed that integrins[15,32] among the favored protein aggregations on nanorods topography are crucial to enhanced MSCs osteogenesis on O-P. Curran et al.[12] reported that –NH_2-modified surfaces could promote osteogenic differentiation of MSCs both under basic and osteogenic stimulated conditions. Therefore, it is concluded that the superiority of OA(S)-P in supporting MSCs osteogenesis depends on both the favorable surface topography and chemistry. In other words, the nanorods topography of OA(S)-P plays a pivotal role in supporting MSCs functions and the chemical modification rendered by NH_3 PIII enhances the positive effects further.

An advantage of this plasma technique is that the structures responsible for the enhanced performance are created intrinsically in the PTFE. Hence, unlike coatings or bound molecules, there is no risk of materials delamination. Figure S4 (Supporting Information) displays the load-displacement curves acquired from the samples. The load segments of all the curves are smooth, providing evidence that no cracking occurs during loading. The process also has other advantages such as low cost, simple operation, robustness, and more importantly, no compromise on the bulk properties of the materials. By using the mesh-assisted approach, a surface area of 6 cm × 7 cm (Figure 1a) or larger can be processed uniformly to meet the requirements for large-area repair. Different functions can be endowed on the same PTFE substrate locally by means of mask shifting. As shown in Figures 1a and 1h, the symmetrical or asymmetrical masks can be imprinted onto the samples to produce different properties. Owing to the ability to obtain different local MSCs responses, this process can be utilized to hierarchically regulate the stem cell fate in different areas on the same substrate and this would be very difficult by many other strategies.

In conclusion, an advanced plasma treatment produces different surface morphology and chemistry on PTFE to direct the adhesion, proliferation, and differentiation of MSCs. In particular, sample OA(S)-P shows the best MSCs proliferation and spontaneous osteogenic differentiation. The nanorods topography on OA(S)-P plays a pivotal role in supporting MSCs functions and the chemical modification rendered by NH_3 PIII enhances the positive effects. Since the structures responsible for the enhanced performance are created in the PTFE,

materials delamination can be circumvented. Because of the ability to obtain locally different MSCs responses, this process can be utilized to hierarchically regulate the stem cell fate in different areas on the same substrate. Large-scale and locally specific features can be produced by this technology which has immense potential in the development of better implant materials.

Experimental Section

Sample Preparation: PTFE (0.25 mm in thickness) purchased from Good Fellow was cut into 9 cm x 9 cm pieces and processed in the Plasma Laboratory, City University of Hong Kong. A detailed description of the PIII setup can be found elsewhere.[18,33] As shown in the schematic diagram (Figure S1, Supporting Information), the high voltage sample stage and supporting voltage feedthrough rod were shielded from the plasma by a metal cage made of stainless steel. A hole (20 cm in diameter) was made in the centre of the top cover. A stainless steel mask with a circular opening (12 cm in diameter) was covered by a stainless steel mesh (120 meshes per inch and 65 μm wire diameter). The PTFE sample was placed 1 cm from the mask.

In addition to conducting oxygen PIII on the PTFE samples, the surface properties of the PTFE were modified using multiple steps in this study. Table 1 presents the different treatment parameters together with the sample designations. U-P denotes the untreated PTFE as the control. Samples O-P and N-P underwent only oxygen or nitrogen PIII, respectively using the parameters (sample bias = –15 kV, pulsing frequency = 500 Hz, and pulse duration = 200 μs). Samples OA(S)-P, NA-P, and HA-P were subjected to dual PIII treatments. OA(S)-P underwent oxygen PIII followed by ammonia PIII with oxygen PIII conducted in the long pulse, high frequency mode (–15 kV, 500 Hz, and 200 μs) and ammonia PIII in the conventional short pulse, low frequency mode (–15 kV, 50 Hz, and 30 μs). Sample NA-P was subjected to nitrogen PIII and then ammonia PIII using the same parameters (–15 kV, 500 Hz, and 200 μs). Sample HA-P underwent hydrogen PIII and subsequent ammonia PIII using the same parameters (–15 kV, 500 Hz, and 200 μs).

Surface Characterization: The samples were dried and sputter-coated with gold prior to SEM examination. The static contact angles were measured by the sessile drop method on a Rame'-Hart instrument (USA) at ambient humidity and temperature when distilled water was used as the medium (10 μL per drop). Each data point represents the average and standard deviation of ten measurements on each specimen for statistical accountability. XPS was conducted on a Physical Electronics PHI 5802 equipped with a monochromatic Al K_α source. A constant pass energy (11.75 eV) was conducted and all the data were collected at a take-off angle of 45° with a step size of 0.1 eV. A colorimetric method using Orange II dye was employed to determine the C=H/C–NH_2 groups on the samples.[34,35] In particular, the 1 cm × 1 cm specimens (three replicates) were immersed in the dye solution (15 mg mL^{-1}, adjusted to a pH of 3 with HCl) at 37 °C for 40 min and then rinsed thrice with the acidic solution (pH 3). After air drying, the stained samples were separately immersed in the alkaline solution (1 mL, adjusted to a pH of 12 with NaOH) for bound dye desorption. Finally, the solution was adjusted to a pH of 3 by HCl (a final volume of 1.5 mL) and the absorbance was measured spectrophotometrically at 484 nm. The surface C=NH/C–NH_2 content is 1:1 proportional to the dye adsorption and expressed in pmol mm^{-2}.

Cell Cultures: MSCs were isolated from bone marrows in the femurs of 2-weeks-old Sprague-Dawley rats and expanded in the α-minimum essential medium (α-MEM, Gibco-BRL) supplemented with 10% fetal bovine serum (FBS, Gibco-BRL), glutamine (292 μg mL^{-1}), penicillin (100 U mL^{-1}), and streptomycin (100 mg mL^{-1}). All the MSCs used in this study were at passage 1. All the samples were cut into 1 cm x 1 cm and 2 cm × 2 cm pieces for the subsequent experiments. Before cell seeding, the substrates were sterilized with 75% alcohol overnight and then rinsed thrice with sterile phosphate-buffered saline (PBS). All the cultures were incubated in a humidified atmosphere of 5% CO_2 at 37 °C and the medium was refreshed every 3 days.

Cell Viability Assay: The MSCs were seeded on 1 cm x 1 cm specimens (four replicates, 1.5 x 10^4 cells per sample) held by 24-well tissue culture plates. After different periods (6 hours for cells adhesion and 1 day, 3 days, 6 days for cells proliferation), the viable cells were quantified by the WST-8 reagent (Donjindo) according to the manufacturer's instructions.

qPCR: qPCR was performed in 2 separate groups. In both groups, the MSCs were plated onto the 2 cm x 2 cm specimens (three replicates, 8 × 10^4 cells per sample) using 6-well tissue culture plates as the holders. In group 1, the substrates seeded were cultured in a basic growth medium for the initial 3 days and then refreshed with the osteogenic medium (basic medium added with 5 μmol mL^{-1} glycerophosphate, 50 μg mL^{-1} ascorbic acid, and 100 pmol mL^{-1} dexamethasone) for up to 10 days. In group 2, the substrates seeded were incubated in a basic growth medium throughout the culturing period (10 days).

After culturing, the total RNA of the cells was extracted by a TRIZOL reagent (Invitrogen) and the cDNA was prepared by a PrimeScript RT reagent Kit (TaKaRa) according to the manufacturer's protocols. Finally, qPCR was performed on the Applied Biosystems 7500 Real Time PCR system by using the SYBR green reagents (TaKaRa). The gene expressions of ALP, BSP, OPN and OCN were analyzed with β-actin serving as the house-keeping gene for normalization. The primer sequences of the genes are shown in Table S1 (Supporting Information). Quantification of the gene expression was based on the comparative cycle-threshold (C_T) method expressed as $2^{-\Delta\Delta C_T \pm SD}$.[36]

Immunofluorescence: After culturing for 14 days in the basic growth medium, the MSCs on the samples (1 cm x 1 cm) were rinsed twice with PBS and fixed in 4% paraformaldehyde/PBS for 20 min at room temperature. After fixing, a permeabilizing buffer (0.2% Triton X-100/PBS) was added for 10 min. The samples were washed twice with PBS and then incubated in 1% bovine serum albumin (BSA)/PBS for 1 h at room temperature, followed by the additions of anti-osteopontin (1:100, AKm2A1, Santa Cruz Biotechnology) and anti-osteocalcin primary antibodies (1:100, AB10911, Millipore) for overnight incubation at 4°C. After incubation and three washes with PBS, the goat anti-mouse IgG-TRITC and goat anti-rabbit IgG-FITC were added for double staining and the cells were incubated for 1 hour at room temperature. Finally, the cells were washed thrice with PBS and stained for 10 min by hoechst (Sigma) for nuclei staining. All the samples were mounted on slides and photographed by a FV1000 confocal microscope (Olympus).

Supporting Information

Supporting Information is available from the Wiley Online Library or from the author.

Acknowledgements

This work was supported by Hong Kong Research Grants Council (RGC) General Research Funds (GRF) No. CityU 112510 and Hong Kong Research Grants Council Special Equipment Grant SEG_CityU05. H. Y. Wang would like to thank Mr. Haiping Sun and Prof. Yumei Zhang (Department of Prosthodontics, School of Stomatology, Fourth Military Medical University) for their technical support.

Received: December 29, 2011
Revised: April 17, 2012
Published online: May 25, 2012

[1] E. Gentleman, R. J. Swain, N. D. Evans, S. Boonrungsiman, G. Jell, M. D. Ball, T. A. V. Shean, M. L. Oyen, A. Porter, M. M. Stevens, *Nature Mater.* **2009**, *8*, 763.

[2] H. P. Yuan, H. Fernandes, P. Habibovic, J. de Boer, A. M. C. Barradas, A. de Ruiter, W. R. Walsh, C. A. van Blitterswijk, J. D. de Bruijn, *Proc. Natl. Acad. Sci. USA* **2010**, *107*, 13614.

[3] M. J. Dalby, N. Gadegaard, R. Tare, A. Andar, M. O. Riehle, P. Herzyk, C. D. W. Wilkinson, R. O. C. Oreffo, *Nature Mater.* **2007**, *6*, 997.
[4] A. Wilkinson, R. N. Hewitt, L. E. McNamara, D. McCloy, R. M. D. Meek, M. J. Dalby, *Acta Biomater.* **2011**, *7*, 2919.
[5] M. R. Urist, *Science* **1965**, *150*, 893.
[6] A. Y. Friedens, *Clin. Orthop. Relat. Res.* **1968**, *59*, 21.
[7] N. Jaiswal, S. E. Haynesworth, A. I. Caplan, S. P. Bruder, *J. Cell. Biochem.* **1997**, *64*, 295.
[8] A. M. Mackay, S. C. Beck, J. M. Murphy, F. P. Barry, C. O. Chichester, M. F. Pittenger, *Tissue Eng.* **1998**, *4*, 415.
[9] F. Barry, R. E. Boynton, B. S. Liu, J. M. Murphy, *Exp. Cell Res.* **2001**, *268*, 189.
[10] C. Toma, M. F. Pittenger, K. S. Cahill, B. J. Byrne, P. D. Kessler, *Circulation* **2002**, *105*, 93.
[11] K. Matsushita, Y. J. Wu, Y. Okamoto, R. E. Pratt, V. J. Dzau, *Hypertension* **2002**, *48*, 1095.
[12] J. M. Curran, R. Chen, J. A. Hunt, *Biomaterials* **2006**, *27*, 4783.
[13] D. S. W. Benoit, M. P. Schwartz, A. R. Durney, K. S. Anseth, *Nature Mater.* **2008**, *7*, 816.
[14] A. J. Engler, S. Sen, H. L. Sweeney, D. E. Discher, *Cell* **2006**, *126*, 677.
[15] J. Park, S. Bauer, K. von der Mark, P. Schmuki, *Nano Lett.* **2007**, *7*, 1686.
[16] J. Park, S. Bauer, K. A. Schlegel, F. W. Neukam, K. von der Mark, P. Schmuki, *Small 2009*, *5*, 666.
[17] S. Oh, K. S. Brammer, Y. S. J. Li, D. Teng, A. J. Engler, S. Chien, S. Jin, *Proc. Natl. Acad. Sci. USA* **2009**, *106*, 2130.
[18] H. Y. Wang, D. T. K. Kwok, W. Wang, Z. W. Wu, L. P. Tong, Y. M. Zhang, P. K. Chu, *Biomaterials* **2010**, *31*, 413.
[19] H. C. Tenenbaum, J. N. M. Heersche, *Calcif. Tissue Int.* **1982**, *34*, 76.
[20] Y. Liu, P. R. Cooper, J. E. Barralet, R. M. Shelton, *Biomaterials* **2007**, *28*, 1393.
[21] Y. Ogata, *J. Periodontal Res.* **2008**, *43*, 127.
[22] D. T. Denhardt, X. J. Guo, *FASEB J.* **1993**, *7*, 1475.
[23] T. A. Owen, M. Aronow, V. Shalhoub, L. M. Barone, L. Wilming, M. S. Tassinari, M. B. Kennedy, S. Pockwinse, J. B. Lian, G. S. Stein, *J. Cell. Physiol.* **1990**, *143*, 420.
[24] P. Ducy, C. Desbois, B. Boyce, G. Pinero, B. Story, C. Dunstan, E. Smith, J. Bonadio, S. Goldstein, C. Gundberg, A. Bradley, G. Karsenty, *Nature* **1996**, *382*, 448.
[25] J. H. Zhang, X. J. Yu, H. D. Li, X. H. Liu, *Appl. Surf. Sci.* **2002**, *185*, 255.
[26] M. Adami, L. Guzman, B. Y. Man, A. Miotello, P. M. Ossi, *Thin Solid Films* **2004**, *459*, 318.
[27] H. Dong, T. Bell, *Surf. Coat. Tech.* **1999**, *111*, 29.
[28] U. Lappan, U. Geissler, U. Scheler, *Macromol. Mater. Eng.* **2007**, *292*, 641.
[29] X. J. Feng, L. Jiang, *Adv. Mater.* **2006**, *18*, 3063.
[30] G. Kaur, M. T. Valarmathi, J. D. Potts, E. Jabbari, T. Sabo-Attwood, Q. Wang, *Biomaterials* **2010**, *31*, 1732.
[31] G. Kaur, C. Wang, J. Sun, Q. Wang, *Biomaterials* **2010**, *31*, 5813.
[32] J. Takagi, B. M. Petre, T. Walz, T. A. Springer, *Cell* **2002**, *110*, 599.
[33] D. T. K. Kwok, H. Y. Wang, Y. M. Zhang, K. W. K. Yeung, P. K. Chu, *J. Appl. Phys.* **2009**, *105*, 053302.
[34] E. Uchida, Y. Uyama, Y. Ikada, *Langmuir* **1993**, *9*, 1121.
[35] S. Noel, B. Liberelle, L. Robitaille, G. De Crescenzo, *Bioconjugate Chem.* **2011**, *22*, 1690.
[36] K. J. Livak, T. D. Schmittgen, *Methods* **2001**, *25*, 402.

ADVANCED MATERIALS

Supporting Information

for *Adv. Mater.*, DOI: 10.1002/adma. 201104967

Tailoring of Mesenchymal Stem Cells Behavior on Plasma-Modified Polytetrafluoroethylene

*Huaiyu Wang , Dixon T. K. Kwok , Ming Xu , Haigang Shi , Zhengwei Wu , Wei Zhang , and Paul K. Chu **

Submitted to ADVANCED MATERIALS

DOI: 10.1002/adma. 201104967

Tailoring of Mesenchymal Stem Cells Behavior on Plasma-Modified Polytetrafluoroethylene

By *Huaiyu Wang, Dixon T. K. Kwok, Ming Xu, Haigang Shi, Zhengwei Wu, Wei Zhang,* and *Paul K. Chu**

[*] Dr. H. Y. Wang, Prof. P. K. Chu, Dr. D. T. K. Kwok, Dr. M. Xu, Dr. Z. W. Wu
Department of Physics & Materials Science, City University of Hong Kong
Tat Chee Avenue, Kowloon, Hong Kong, China
E-mail: (paul.chu@cityu.edu.hk)
Dr. Z. W. Wu
Department of Modern Physics, University of Science and Technology of China
Hefei, Anhui, 230026, China
Mr. H. G. Shi, Dr. W. Zhang
Technical Institute of Physics and Chemistry, Chinese Academy of Sciences
Beijing, 100080, China

Keywords: (plasma immersion ion implantation, polytetrafluoroethylene, surface properties, mesenchymal stem cells, osteogenic differentiation)

Supporting Information

Table S1. Sequences of the primers.

Gene	Primers [5'-3']	Amplicon
ALP [NM_022665.3]	F: ATGTCAACCGAAACGCCTCAG R: ATGGCGGAGTCGAACATGGCA	185bp
BSP [NM_012587.2]	F: TGTGGAATGGTGCTACGGTCTC R: GATCAACAGCCCTGATTTACGATG	173bp
OPN [XM_002728077]	F: AGACCATGCAGAGAGCGAG R: ACGTCTGCTTGTGTGCTGG	105bp
OCN [NM_013414.1]	F: TGCAAAGCCCAGCGACTCT R: AGTCCATTGTTGAGGTAGCG	99bp
β-actin [NM_031144]	F: GGAGCCAGGGCAGTAATCT R: CGTTGACATCCGTAAAGACC	108bp

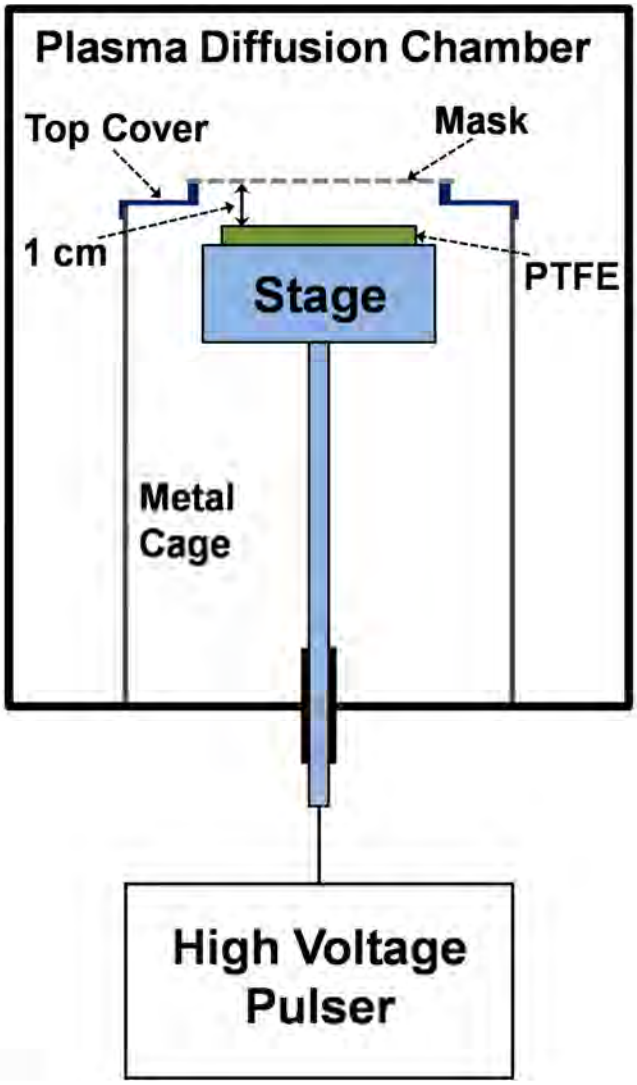

Figure S1. Schematic diagram of the customized plasma immersion ion implantation (PIII) setup.

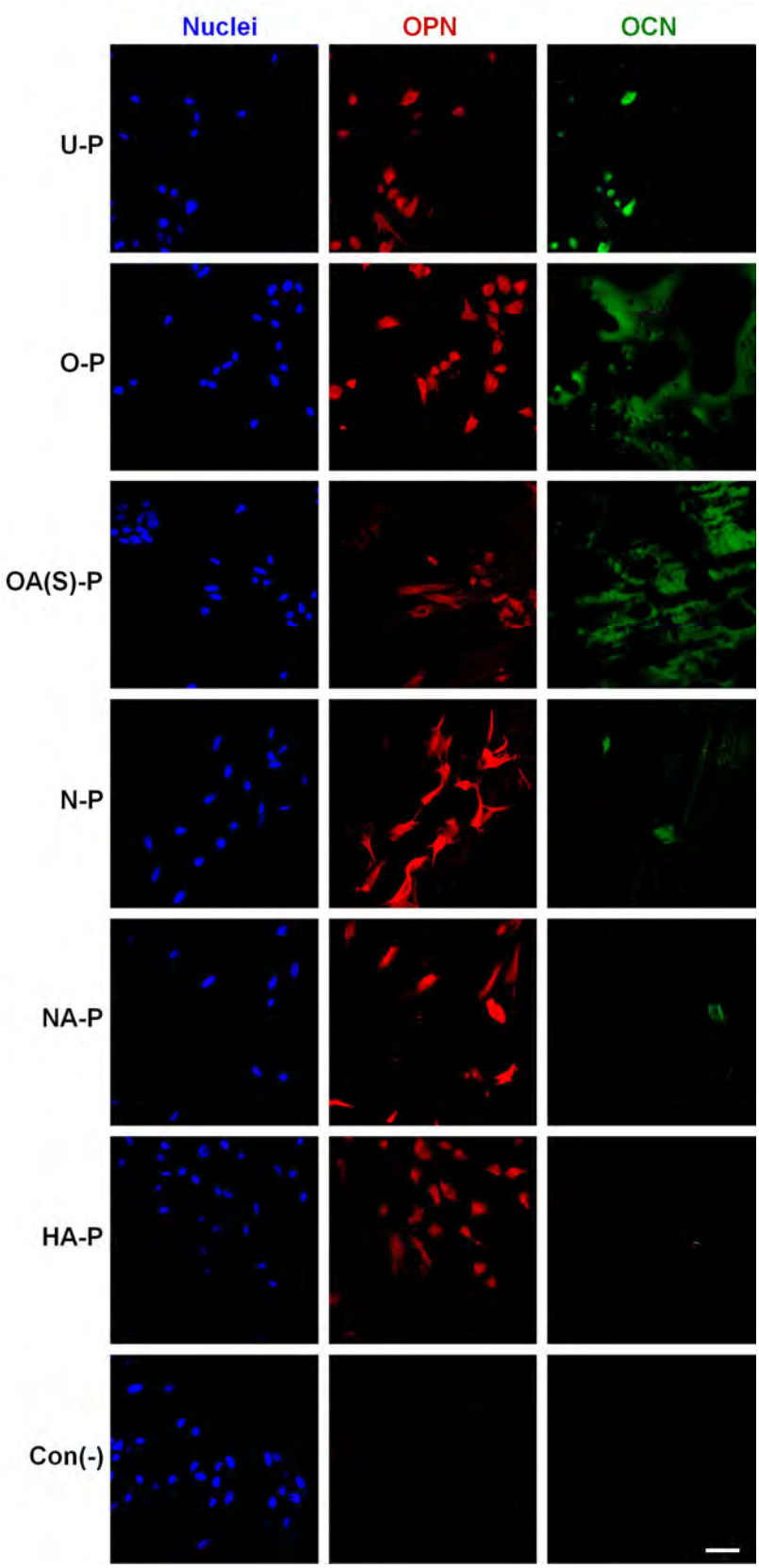

Figure S2. Immunofluorescent images of MSCs for OPN (center column) and OCN (right column) as well as hoechst staining (left column) after culturing for 14 days in a basic growth medium (scale bar is 100 μm).

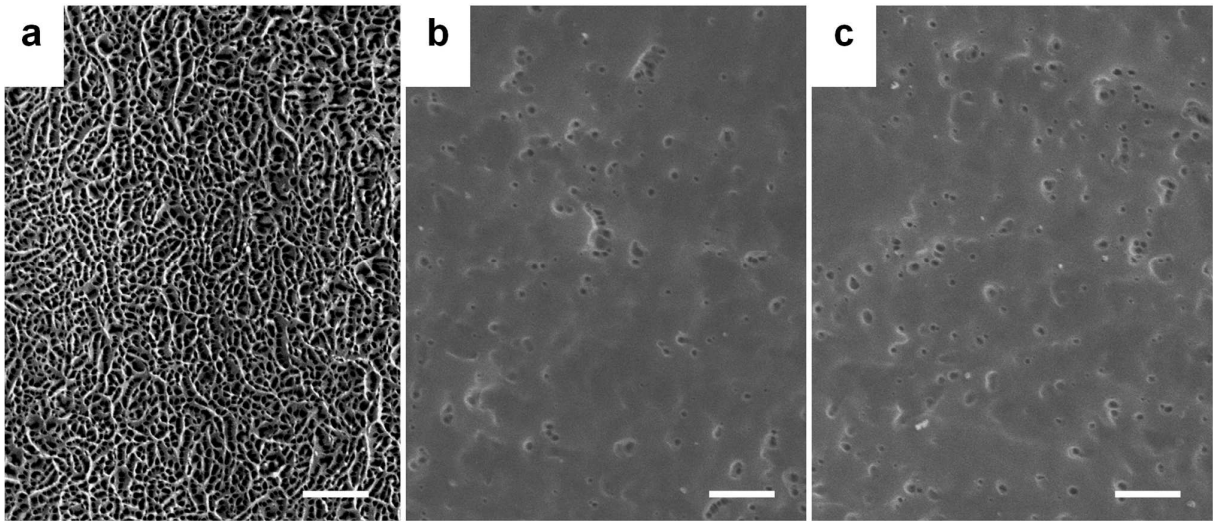

Figure S3. SEM micrographs (top view) of PTFE samples after long pulse, high frequency: (a) O_2/NH_3 PIII, (b) H_2 PIII, and (c) NH_3 PIII (scale bar is 2 μm).

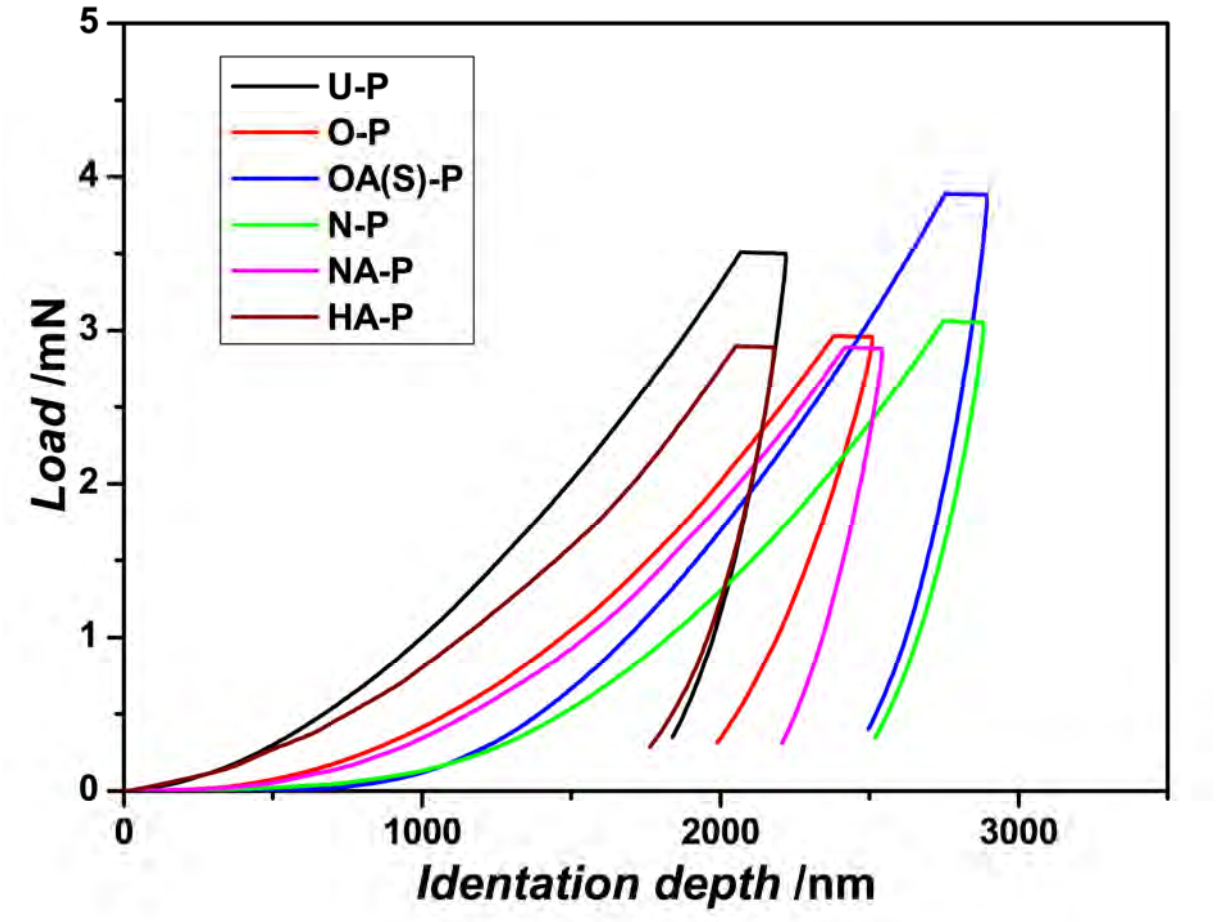

Figure S4. Load-displacement curves acquired from the various samples.